Atmos. Chem. Phys. Discuss., 10, 20125–20165, 2010
www.atmos-chem-phys-discuss.net/10/20125/2010/
doi:10.5194/acpd-10-20125-2010

Atmospheric Chemistry and Physics Discussions

Evaluation of simulated photochemical partitioning of oxidized nitrogen in the upper troposphere

B. H. Henderson[1,2], R. W. Pinder[2], J. Crooks[2], R. C. Cohen[3], W. T. Hutzell[2], G. Sarwar[2], W. S. Goliff[4], W. R. Stockwell[5], A. Fahr[5], R. Mathur[2], A. G. Carlton[2], and W. Vizuete[1]

[1]Department of Environmental Science and Engineering, University of North Carolina, Chapel Hill, NC, USA
[2]National Exposure Research Laboratory, US Environmental Protection Agency (USEPA), RTP, NC, USA
[3]Departments of Chemistry and Earth and Planetary Sciences, University of California, Berkeley, CA, USA
[4]College of Engineering-CERT, University of California at Riverside, Riverside, CA, USA
[5]Department of Chemistry, Howard University, Washington, DC, USA

Received: 7 August 2010 – Accepted: 12 August 2010 – Published: 25 August 2010

Correspondence to: B. H. Henderson (barronh@gmail.com)

Published by Copernicus Publications on behalf of the European Geosciences Union.

Abstract

Regional and global chemical transport models underpredict NO_x ($NO+NO_2$) in the upper troposphere where it is a precursor to the greenhouse gas ozone. The NO_x bias been shown in model evaluations using aircraft data (Singh et al., 2007) and total column NO_2 (molecules cm^{-2}) from satellite observations (Napelenok et al., 2008). The causes of NO_x underpredictions have yet to be fully understood due to the interconnected nature of simulated emission, transport, and chemistry processes. Recent observation-based studies suggest that, in the upper troposphere, simulated chemistry overpredicts hydrogen radicals ($OH^\bullet$ and $HO_2^\bullet$) and would convert NO_x to HNO_3 too quickly (Olson et al., 2006; Bertram et al., 2007; Ren et al., 2008). Since typical chemistry evaluation techniques are not available for upper tropospheric conditions, this study develops an evaluation platform from in situ observations, stochastic convection, and deterministic chemistry. We derive a stochastic convection model and optimize it using two simulated datasets of time since convection, one based on meteorology and the other on chemistry. The chemistry surrogate for time since convection is calculated using seven different chemical mechanisms, all of which predict shorter time since convection than our meteorological analysis. We evaluate chemical simulations by inter-comparison and by pairing results with observations based on NO_x:HNO_3, a photochemical aging indicator. Inter-comparison reveals individual chemical mechanism biases and recommended updates. Evaluation against observations shows that all chemical mechanisms overpredict NO_x removal relative to long-lived methanol and carbon monoxide. All chemical mechanisms underpredict observed NO_x by at least 30%, and further evaluation is necessary to refine simulation sensitivities to initial conditions and chemical rate uncertainties.

ACPD
10, 20125–20165, 2010

Title Page
Abstract | Introduction
Conclusions | References
Tables | Figures
◂◂ | ▸▸
◂ | ▸
Back | Close
Full Screen / Esc
Printer-friendly Version
Interactive Discussion

1 Introduction

Total oxidized nitrogen [NO_y=NO+NO_2+NO_3+N_2O_5+HNO_2+HNO_3+HO_2NO_2+$CH_3(CH_2)_nC(O)OONO_2$+RNO_3] includes many compounds with a wide variety of physical properties and environmental roles. Nitrogen oxides (NO_x=NO+NO_2) are water insoluble, chemically reactive in the atmosphere, and serve as precursors to ozone. Peroxy nitrates (PNs=HO_2NO_2+$CH_3(CH_2)_nC(O)OONO_2$) are insoluble, their chemical reactivity is temperature dependent, and they act primarily as a reservoir for NO_x. Nitric acid, on the other hand, is highly water soluble, chemically stable, and is a primary component of acid rain. The partitioning of the NO_y between component compounds is controlled by a mix of physical (i.e., emissions and transport) and chemical (i.e., aqueous, particle, and gas-phase) processes and is critical to accurate simulation of environmental stress. The partitioning between NO_y compounds influences the efficiency of NO_y wet scavenging, the availability of HNO_3 for acid rain, and the amount of NO_x for production of the greenhouse gas ozone. As a greenhouse gas, ozone is 10 times more efficient in the upper troposphere than in the lower troposphere (Lacis et al., 1990). The upper troposphere, with its high ozone mixing ratio and high radiative forcing efficiency, is also where chemical transport models (CTMs) underpredicted the NO_x precursor (Napelenok et al., 2008; Bertram et al., 2007; Singh et al., 2007; Napelenok et al., 2008).

Underprediction of upper tropospheric NO_x could be caused by any of the interrelated chemical and physical processes in CTMs that affect NO_y partitioning. Increasing simulated NO_x from aircraft and lightning increase NO_x mixing ratios, but does not resolve the bias. Pickering et al. (2009) found that lightning improved NO_x, but most bias improvement was below 8 km. Hudman et al. (2007) concluded that lightning emissions improved simulated NO_x mixing ratios, but the median simulated NO_x mixing ratio was still 300 ppt low-biased and the primary chemical sink (HNO_3) was now overpredicted. Other emission studies have quantified NO_x emissions from aircraft (Eyers et al., 2004; Sutkus et al., 2003), which are generally small compared to lightning except perhaps directly in particular flight paths (Hudman et al., 2007). Recent chemistry evaluations suggest that chemical representation could contribute to underpredictions of NO_x via overpredicting HNO_3 formation rates (Olson et al., 2006; Bertram et al., 2007; Ren et al., 2008). Emissions, physics, and chemistry both contribute to the NO_x mixing ratios, requiring evaluation of each process in isolation.

This study develops and implements a new evaluation technique designed to isolate simulated chemistry in the upper troposphere. Chemistry evaluation, to date, uses either smog chamber experiments or quasi-Lagrangian measurements. Smog chamber experiments provide a direct evaluation in a controlled environment, but chamber experiments are carried out at surface level temperatures and pressures ($T \approx 298$ K, $P \approx 1$ atm) and typically high NO_x mixing ratios ($NO_x > 50$ ppb), which are significantly different from the upper troposphere (medians from this study: $T = 240$ K, $P = 0.31$ atm, $NO_x = 0.4$ ppb). Quasi-Lagrangian aircraft measurements can provide temperature/pressure appropriate time-series case studies, but the Lagrangian nature of the sampling is often difficult to verify given uncertainty in meteorology (as in Real et al., 2008). Smog chamber evaluations do not have appropriate environmental conditions, and quasi-Lagrangian sampling does not provide enough high-quality samples for statistical evaluation. Any upper tropospheric evaluation must account for both environmental conditions and air parcel interaction with meteorology.

We propose a statistically robust chemical evaluation using in situ upper tropospheric aircraft observations from the Intercontinental Chemical Transport Experiment (INTEX-NA; Singh et al., 2006). Although these aircraft measurements do not sample a single air parcel through space and time, the measurements can be grouped and sorted by photochemical age using a technique developed by Bertram et al. (2007). This technique assumes that the “youngest” air parcels are the result of deep convection events. Deep convection mixes air from the earth’s surface into the upper troposphere and is generally associated with precipitation that removes water soluble HNO_3, but not less soluble NO_x. Thus air parcels immediately following convection have very high ratios of NO_x:HNO_3. After deep convection, air parcels undergo chemical processing that con-

ACPD
10, 20125–20165, 2010

verts NO_x to HNO_3, reducing the NO_x:HNO_3 ratio until the air parcel is removed from the upper troposphere by convective downdrafts. Initial deep convection is identified by high NO_x:HNO_3 and subsequent downdrafts can be handled stochastically. Therefore, the observed NO_x:HNO_3 ratio provides a relative metric of time since convection that can be used to create a time-series. This time-series is suitable for evaluating chemistry in the upper troposphere because it has appropriate environmental conditions and enough observations for statistical evaluation.

This study uses a relative time-series of observations to evaluate photochemical aging predicted by seven different chemistry representations. Each chemistry representation, called a chemical mechanism, uses reaction sets with varying degrees and methods of simplification (Dodge, 2000). We selected seven chemical mechanisms from chemical transport models with spatial scales ranging from point to global. The complexity of each chemical mechanism also ranges from near-explicit to condensed. Near-explicit chemical mechanisms represent all known chemical compounds and reactions. Although all known reactions are included, many reactions have large uncertainty in the rate coefficient and stoichiometric yield. Condensed mechanisms use abstractions to reduce the computational load, but often include empirical tuning for conditions that may limit the applicability of the mechanism to all environmental conditions.

We evaluate each chemical mechanism to test three main questions. First, is the rate of chemical aging consistent between chemical mechanisms and observations? Second, are biases consistent for all chemical mechanisms, and therefore, fundamental to the state of the science, or can mechanism differences identify misrepresentations? Third, to what extent can chemical mechanisms' photochemical aging cause under-prediction of NO_2? Finally, we evaluate factors that contribute to partitioning biases for total oxidized nitrogen in an attempt to improve the individual chemical mechanisms.

ACPD
10, 20125–20165, 2010
Upper tropospheric NO_y evaluation
B. H. Henderson et al.

2 Methods

2.1 Modeling framework

This study simulates photochemical aging and physical processing of air parcels following deep convection. Deep convection mixes lower tropospheric air with VOCs and NO_x into upper tropospheric air (Bertram et al., 2007). Deep convection produces clouds that scavenge water soluble HNO_3 and lightning that produces NO_x. These two processes result in high NO_x:HNO_3 ratios that can identify air parcels transported by recent convection. After convection, the air parcel photochemically ages, converting NO_x to HNO_3, and mixes with background upper tropospheric air until downdrafts associated with subsequent deep convection remove air parcels from the upper troposphere. Particle chemistry is most likely of limited importance in our study due to low particle concentrations and subsequent low total particle surface area. Aircraft observe air parcels at varying time since convection and, therefore, with varying extents of photochemical aging. We then developed a model to reproduce the observed distribution of photochemical age. To reproduce the distribution of air parcels, our model framework simulates gas-phase chemistry, photolysis, mixing into background air (i.e., dilution, dispersion, diffusion), and subsequent convection. Subsequent convection is caused by meteorological processes external to our box model, and we simulate this process stochastically using a distribution of time between convective influence. First, we simulate 10 d of chemical aging, or air parcel lifetime, for a variety of physical and chemical conditions representative of recently convected air parcels in the INTEX-NA observational database. In the real environment, we expect that air parcel lifetimes have a distribution that is governed by subsequent convection. We stochastically simulate subsequent convection by optimizing the distribution of air parcel lifetimes for consistency with observed chemical mixing ratios. The air parcel lifetimes can be evaluated against the empirical distribution, and the predicted distribution of chemical species during the air parcel lifetime can be compared to observed mixing ratios.

ACPD
10, 20125–20165, 2010

2.2 Observations

Aircraft observations provide box model initial conditions and photochemical age needed for model evaluation. We first sorted observations using NO_x:HNO_3 as a chemical indicator of photochemical age. The measurements with the highest NO_x:HNO_3 ratios provide physical conditions and initial chemical mixing ratios for model simulations using seven chemical mechanisms. The predictions are then evaluated against the observational time-series to assess the performance of simulated chemistry.

We use aircraft observations from the National Aeronautics and Space Administration (NASA) DC-8 aircraft flights during Intercontinental Chemical Transport Experiment – North America (INTEX-NA) campaign (Singh et al., 2006). We started with the 10-s averaged NASA DC-8 observation database (n=56465). We then filtered the observation database to include only measurements of the upper troposphere (8 km<altitude<10 km). We exclude air parcels with any fractional cloud presence that would have active wet scavenging, which would influence NO_x:HNO_3. We also removed air parcels that might have been influenced by stratospheric intrusion (H_2O<200 ppb or ^{7}Be:^{210}Pb>1000) or biomass burning (CH_3CN>200 ppt). The remaining observations fall into two distinct groups: those influenced by polluted air (CO≥80 ppb) and those influenced by background air (CO<80 ppb) (Singh et al., 2007). Our analysis has been performed with both polluted and background influenced observations and excluding background observations. Both analyses give similar results. In this study, we focused on the influence of polluted air and include only those air parcels with over 80 ppb CO (n=861). These observations represent upper troposphere air parcels with varying photochemical age.

The upper troposphere observations are then divided into age groups according to photochemical age as assessed by NO_x:HNO_3. The observed NO_x:HNO_3 ratio in our filtered dataset is log-normally distributed, and we split observations into 4 age groups that are non-overlapping, have comparable sample sizes, and capture the range of air parcel aging. The age groups, which represent relative photochemical age, will

ACPD
10, 20125–20165, 2010

be referred to as *fresh*, *young*, *midage*, or *old*. Each category has a minimum of 215 observations (*fresh*: 216, *young*: 215, *midage*: 215, *old*: 215). An additional classification, "initial", was added to capture immediate convection for model initialization. The *initial* age group includes the youngest 50% of the *fresh* observations and represents air parcels that have been convected most recently. Figure 1 shows the total oxidized nitrogen (NO_y) partitioning of each age group and shows that only NO_x and HNO_3 have age-dependent mixing ratios.

2.3 Box model

We use a common box model framework for all simulations to remove artifacts of multiple modeling systems and isolate differences between seven chemical mechanisms. The use of a common box model removed variability in ordinary differential equation solvers and physical representations. The Dynamically Simple Model of Atmospheric Chemical Complexity (DSMACC) provided the flexibility and power necessary to model all our chemical mechanisms. The DSMACC model (Emmerson and Evans, 2009) is based on the Kinetic Pre-Processor (KPP) (Sandu and Sander, 2005), which has a flexible rate coefficient representation. The flexible rate representation allowed all seven chemical mechanisms to use their native reaction rate coefficient forms. We have added a mixing process to the DSMACC model to account for dilution, dispersion, and diffusion. Air parcels mix in "background" air where each chemical species mixing ratio is the mean of observations described above. The "background" air includes air parcels influenced by both polluted and background air. The rate of mixing is assumed to be constant and set to 5% per day (Bertram et al., 2007). Sensitivity analysis using up to 10 times the mixing rate did not yield meaningfully different results (see Fig. 10). This box model represents *only* gas-phase chemical reactions and mixing with background air; there is no particle or aqueous chemistry.

ACPD
10, 20125–20165, 2010

2.4 Gas-phase chemistry

This study evaluates gas-phase chemistry from seven chemical mechanisms that each have different research goals. Carbon Bond version 2005 (Yarwood et al., 2005) and the State Air Pollution Research Center '99 (SAPRC99) (Carter, 2000) are typically used for urban to continental simulation. In addition, SAPRC '07 (Carter, 2009) and Regional Atmospheric Chemical Mechanism version 2 (RACM2) (Stockwell et al., 2008; Goliff and Stockwell, 2008; Goliff et al., 2010) are mechanisms that are planned to be included in the Environmental Protection Agency's Community Multiscale Air Quality model. The Goddard Earth Observing System-Chemistry (GEOS-Chem) (Mao et al., 2009) and Model for OZone And Related chemical Tracers (MOZART-4) (Emmons et al., 2010) are typically used for global simulation. The near-explicit LEEDS Master Chemical Mechanism (MCM) (Saunders et al., 1997) is typically used in box model or trajectory simulations. For MCM, we extracted only those chemical reactions that would be active given our initial conditions and subsequent chemical products. The seven chemical mechanisms we evaluate are used for a range of research goals and have a range of computational complexity (see reactions and species in Table 1).

2.5 Photolysis

Gas-phase chemistry simulations typically use different photo-dissociation models that strongly influence radical initiation and photochemical cycling. Each chemical mechanism evaluated in this study is typically used in a host chemical transport model (i.e., CMAQ, GEOS-Chem, MOZART4, and SBOX) with specific photolysis models to calculate photo-dissociation rates. For example, Carbon Bond and SAPRC chemical mechanisms both used the CMAQ photolysis preprocessor (JPROC), GEOS-Chem used FAST-J photolysis (Wild et al., 2000), MCM used the Tropospheric Ultraviolet model (TUV) version 4.2 (Madronich, 2002), RACM2 used a predecessor of TUV, and MZ4 used TUV version 4.6. Not all photolysis models have implemented pressure/temperature sensitivities and the resulting difference in photolysis rates dominated

ACPD
10, 20125–20165, 2010

the nitrogen partitioning in our initial tests. Particularly, representation of carbonyl photolysis temperature/pressure dependence led to differences in PAN predictions and the representation of near-IR photolysis ($0.00001\,s^{-1}$ Murphy et al., 2004) of pernitric acid led to diverse predictions. The different photolysis rates were not a function of chemical mechanism, but rather of the photolysis model calculation. To truly focus on chemical mechanism differences, the photolysis rates were standardized using TUV v4.6 with modifications consistent with those used in DSMACC for MCM with one exception. All mechanisms except MCM had photolysis reactions for PAN and HO_2NO_2 and, for this analysis, PAN and HO_2NO_2 photolysis has been added to MCM.

2.6 Base simulations

Each chemical mechanism simulates chemical aging for each *initial* observed air parcels (n_i=108). The *initial* air parcels were used as the initialization of all simulated physical and chemical conditions (see Table 2). The *initial* observations of chemical species were mapped to their appropriate chemical mechanism species. Where particular chemical compound measurement was not concurrently available, the median of all *initial* values for that compound was used. An additional simulation was generated using the *initial* age group median value of every chemical compound. Each chemical mechanism was used to simulate 10 d of chemical processing for each *initial* air parcel and the *median* air parcel (n_s=n_i+1). Nighttime simulation results (i.e., solar zenith angles, θ, higher than 75 degrees) are ignored to be consistent with exclusively daytime observations (i.e., $8<\theta<75^{\circ}$).

2.7 Stochastic convection model description

Our simulations must take into account the frequent exchange between the upper and lower troposphere by convection due to cold or warm fronts. Convective updrafts loft air parcels into the upper troposphere which later subside in convective downdrafts from the same, or subsequent frontal system. The time between convective lofting and subsidence, hereafter air parcel lifetime τ_{air}, creates a distribution of time since convection Pr(t) defined by the frequency of frontal systems. To accurately represent observed upper tropospheric air parcels, we must derive the distribution of time since convection Pr(t) and subset our simulation results accordingly. We estimate the distribution of time since convection using a maximum likelihood technique with one stochastic model and two observationally-derived datasets of time since convection.

The stochastic model for the distribution of air parcel lifetimes and of time since convection Pr(t) are both exponential. From an air parcel's perspective, encountering a downdraft is a random and time independent event that will have an exponential distribution (Gallager, 1996). If the INTEX-NA observations were an unbiased random sample, Eq. (1) would describe the distribution of observed time since convection, where $\overline{\tau_{air}}$ is the mean air parcel lifetime. The INTEX-NA observations, however, preferentially sampled air parcels with time since convection less than 6 h (Bertram et al., 2007). To correct for preferential sampling, Eq. (2) doubles the probability of sampling young ($t<6$ h) air parcels (real or simulated), and still has only one fitting parameter $\overline{\tau_{air}}$.

$$\Pr(t) = \frac{1}{\overline{\tau_{air}}} \exp\left(\frac{-t}{\overline{\tau_{air}}}\right) \tag{1}$$

$$\Pr(t) = \begin{cases} \dfrac{1}{\kappa\left(2-\exp\left(\frac{-6}{\overline{\tau_{air}}}\right)\right)} \exp\left(\frac{-t}{\kappa}\right) & \text{if } t \le 6 \\ \dfrac{1}{\overline{\tau_{air}}\left(2-\exp\left(\frac{-6}{\overline{\tau_{air}}}\right)\right)} \exp\left(\frac{-t}{\overline{\tau_{air}}}\right) & \text{if } t > 6 \end{cases} \tag{2}$$

$$\text{where } \kappa = \frac{-6}{\log\left(2\exp\left(\frac{-6}{\overline{\tau_{air}}}\right)-1\right)} \text{ and } \overline{\tau_{air}} \ge 9$$

We estimate $\overline{\tau_{air}}$ by fitting our statistical models (Eqs. 1 and 2) to two empirical estimates of INTEX-NA observed time since convection. First, we use back trajectory

Discussion Paper | Discussion Paper | Discussion Paper | Discussion Paper |

ACPD
10, 20125–20165, 2010

Upper tropospheric NO_y evaluation

B. H. Henderson et al.

encounters with convection systems calculated by Fuelberg et al. (2007). Second, we use our statistical model with chemical mechanisms to reproduce NO_x:HNO_3, a chemical indicator of time since convection. These two approaches, described in detail below, require different assumptions, rely on different models, and provide independent estimates of estimate $\overline{\tau_{air}}$.

Fuelberg et al. (2007) simulated back trajectories and estimated time since convection, which we use to optimize our statistical model. Fuelberg et al. (2007, Table 3) reported the cumulative distribution function (CDF) of time since convection event at intervals starting at 6 h, and ending at 240 h. At 240 h, 91.8% of observations had encountered convection, which leaves 8.2% of observations with unknown time since convection. As a conservative approach, we fit our time since convection model to both the reported and renormalized CDF and provide the range of results as the back trajectory estimate of $\overline{\tau_{air}}$. For both the original and renormalized dataset, we find the $\overline{\tau_{air}}$ (between 1 and 240 h) that minimizes the sum of squared prediction error.

Chemical indicators of time since convection, such as NO_x:HNO_3, provide a second dataset for determining $\overline{\tau_{air}}$. The chemical evolution of NO_x:HNO_3 is reproducible by chemical simulations, using chemical mechanisms, and then subsetting results proportional to Eq. (2). We iteratively subset our base simulations according to the probability of time since convection for each possible $\overline{\tau_{air}}$ (1–240 h). To maximize the size of each subset, we normalize the probability of time since convection to a percentage (exponential: Eq. 3, bias-corrected: Eq. 4) of simulations at each model output time. Each result subset is an ensemble of simulated NO_x:HNO_3 with varying initial conditions and time since convection. We then selected the optimal $\overline{\tau_{air}}$ based on the agreement of the simulation ensemble NO_x:HNO_3 with observed NO_x:HNO_3.

$$p(t) = \exp\left(\frac{-t}{\overline{\tau_{air}}}\right) \tag{3}$$

$$p(t) = \begin{cases} \exp\left(\frac{-t}{\kappa}\right) & \text{if } t \leq 6 \\ \frac{\kappa}{\overline{\tau_{air}}} \exp\left(\frac{-t}{\overline{\tau_{air}}}\right) & \text{if } t > 6 \end{cases} \tag{4}$$

ACPD
10, 20125–20165, 2010
Upper tropospheric NO_y evaluation
B. H. Henderson et al.

where $\kappa = \dfrac{-6}{\log\left(2\exp\left(\frac{-6}{\overline{\tau_{air}}}\right)-1\right)}$ and $\overline{\tau_{air}} \geq 9$

For each $\overline{\tau_{air}}$, we then evaluate the agreement of the simulation ensemble with observed NO_x:HNO_3 using the non-parametric Anderson-Darling K-sample goodness-of-fit statistic (Scholz and Stephens, 1987). The Anderson-Darling test makes no assumptions about data distribution (i.e., skew, kurtosis, etc.), and is particularly sensitive on tails of data distributions. Further, the fit criterion (A^2_{kaN}) is inversely proportional to goodness-of-fit, which makes it ideal for optimization. For each chemical mechanism, we minimize the fit criterion to identify the optimal $\overline{\tau_{air}}$.

2.8 Evaluation approach

We derive $\overline{\tau_{air}}$ using one approach that relies on back trajectory simulation and another that depends on chemical simulation. Using the back trajectory dataset provides an estimate of $\overline{\tau_{air}}$ that depends on the accuracy of a meteorology model. Using the chemical mechanism approach provides an estimate of $\overline{\tau_{air}}$ that depends on the modeled NO_x to HNO_3 conversion. If these two approaches confirm each other, we gain confidence that the chemical mechanisms are photochemically aging at the same rate as observations. If these two approaches conflict, we further evaluate chemical simulation results for evidence that the chemical aging rate is consistent or inconsistent with observed mixing ratios.

We evaluate simulation results, sampled by optimal $\overline{\tau_{air}}$, to test the consistency of chemical aging precursors and products. Chemical aging, here assessed by NO_x:HNO_3, includes the net production or loss of all oxidation precursors and products. If the chemical aging is consistent with observations, other oxidation precursors and products should also be correctly predicted. Our null hypothesis is that, given the same amount of nitrogen oxidation, simulated and observed mixing ratios will be statistically similar for chemical species that were not used to optimize $\overline{\tau_{air}}$. The predicted distributions of mixing ratios for simulated and observed chemical species are statistically compared using a Mann-Whitney-Wilcoxon rank sum test (hereafter rank sum test) (Mann and Whitney, 1947). The rank sum test compares the entire distribution (i.e., not just the mean, median or mode) to test if one is statistically greater than the other. The rank sum test is a non-parametric test and, as such, makes no assumptions about data distribution (i.e., skew, kurtosis, etc). There is no perfect comparison between simulated and measured chemical mixing ratios. For instance, the aircraft observations are time (10 s) and space (1.5 to 3 km) averaged while predictions are instantaneous. The averaging of observations could smooth out some extremes; this is especially true for fast reacting radical species (Olson et al., 2006). To account for some anticipated variation, this study requires a very high degree of confidence to conclude that observations are distinct from model mixing ratios. We only reject the null hypothesis if the probability of the difference in distributions is less than 0.01% ($p<0.0001$).

3 Results

3.1 Stochastic convection: back trajectory results

The back trajectory estimation technique has four discrete estimates of mean air parcel lifetime ($\overline{\tau_{air}}$). Each estimate comes from combining a time since convection dataset, either the unadjusted or renormalized, and a statistical model, either the exponential (Eq. 1) or bias-corrected (Eq. 2) as described in the Stochastic Model Description. Figure 2 shows that renormalizing the back trajectory dataset shortens the $\overline{\tau_{air}}$ estimate, while using the bias-corrected statistical model lengthens the $\overline{\tau_{air}}$ estimate. Both the renormalized dataset and the bias-corrected statistical model incrementally improve the coefficient of correlation (R^2). Using the unadjusted back trajectory results, the exponential model (A) predicts $\overline{\tau_{air}}$=40 h and our bias-corrected model (B) predicts $\overline{\tau_{air}}$=51 h. With renormalized back trajectory results, the exponential model (C) predicts

ACPD
10, 20125–20165, 2010

$\overline{\tau_{\text{air}}}$=47 h and our bias-corrected model (D) predicts $\overline{\tau_{\text{air}}}$=58 h.

3.2 Stochastic convection: NO_x:HNO_3 results

The chemical mechanism technique of estimating of $\overline{\tau_{\text{air}}}$ consistently yielded shorter $\overline{\tau_{\text{air}}}$ values than the back trajectory approach. Figure 3 compares the back trajectory and chemical mechanism $\overline{\tau_{\text{air}}}$. The shortest $\overline{\tau_{\text{air}}}$ estimates for all chemical mechanisms was derived using the exponential model (18–23 h). When using the optimized exponential model (Eq. 3), all chemical mechanisms, except SAPRC99 and RACM2, predicted NO_x:HNO_3 ratios that are statistically different from observations. When the convection model is corrected for sampling bias (Eq. 4), estimated air parcel lifetimes are longer (28–34 h) and NO_x:HNO_3 compares better with observations. When correcting for sampling bias, Fig. 4 shows that all the chemical mechanisms capture the general shape of the observed NO_x:HNO_3. As a result, the Anderson-Darling goodness-of-fit test cannot reject the null hypothesis that NO_x:HNO_3 is consistent with observations (α<0.01). Even though the chemical mechanisms capture the distribution of observed NO_x:HNO_3, the highest $\overline{\tau_{\text{air}}}$ estimate is 6 h shorter than the shortest back trajectory estimate.

The back trajectory estimates of time since convection are all longer than any estimate by chemical mechanisms. If any of the back trajectory $\overline{\tau_{\text{air}}}$ estimates are correct, all of the chemical mechanisms too rapidly remove NO_x. Because NO_x components NO and NO_2 are in steady state, this leads to an underprediction of NO_2. We estimate the NO_2 low-bias by sampling simulated results using our statistical model of convection optimized with back trajectory time since convection. Even when we sample the simulation results using the lowest $\overline{\tau_{\text{air}}}$ estimate (40 h), we underpredict NO_2 by at least 30%.

ACPD
10, 20125–20165, 2010

3.3 Chemical mixing ratio evaluation

The chemical mechanism and back trajectory $\overline{\tau_{\mathrm{air}}}$ estimates disagree, suggesting a need to further evaluate predicted oxidation precursors and products. We evaluate oxidation precursors and products to assess our confidence in the chemical mechanism estimate and to understand chemical mechanism differences. For the chemical evaluation, we use the bias-corrected convection (Eq. 4) because it produces the longest $\overline{\tau_{\mathrm{air}}}$ and, therefore, is the most conservative comparison. Figure 5 overlays simulation ensemble predictions over observations for selected chemical species illustrating chemical mechanism biases. For each chemical species, Fig. 5 shows the distribution of predictions and observations for the five age groups. Figure 5 also denotes observed statistically significant trends between age groups and statistically significant biases in chemical mechanism predictions (see caption for details). For each chemical mechanism, the median is a circle that is hollow when simulations are statistically biased compared to observations. The statistical biases demonstrate that some problems are mechanism-specific, while others affect all tested mechanisms.

Given the same amount of nitrogen aging or oxidation, we expect other oxidation products to compare well. The oxidation products ozone and hydrogen peroxide, however, were only well-predicted until the *midage* age group. For ozone, SAPRC99 underpredicts *midage* and *old* mixing ratios. For hydrogen peroxide, SAPRC99, SAPRC07, and GEOS-Chem underpredict as early as the *midage* age group. By the *old* age group, all chemical mechanisms now under-predict hydrogen peroxide.

Given the same amount of nitrogen aging, we also expect oxidation precursors to compare well. Chemical mechanisms, however, tended to underpredict quickly-reacting carbonyls acetaldehyde (CH_3CHO) and peroxy acetic acid ($CH_3C(O)OOH$) while overpredicting longer-lived species carbon monoxide (CO) and methanol (CH_3OH). Acetaldehyde observations, for example, showed no statistical trend, but the predicted mixing ratios decrease with time. All chemical mechanisms underpredict the acetaldehyde magnitude and inter-quartile range almost immediately. Peroxy

ACPD
10, 20125–20165, 2010

Upper tropospheric NO_y evaluation

B. H. Henderson et al.

acetic acid observations also had no statistically significant decrease with time, but predictions bias depended on the chemical mechanism. For peroxy acetic acid mixing ratios, the SAPRC99 mechanism overpredicted, SAPRC07, RACM2 and GEOS-Chem underpredicted, while MZ4 and CB05 performed statistically well. For longer lived carbon monoxide and methanol, all chemical mechanisms overpredicted as early as the *young* age group.

These long-lived species, particularly methanol (CH_3OH) and carbon monoxide (CO), are important because they are alternative indicators of time. Methanol and carbon monoxide are lost exclusively by slow, well-known $OH^\bullet$ reactions and have relatively little secondary chemical production in the upper troposphere. The bias in predicted carbon monoxide, when NO_x:HNO_3 is used as a surrogate for time, is a clear discrepancy. The chemical mechanisms incrementally remove long-lived carbon as a function of integration time, but as a function of NO_x:HNO_3 there is little integration time difference between age groups. As a result, long-lived carbon is relatively constant between age categories until the parcel is *old*.

3.4 Chemical mechanism biases and recommendations

In several cases, chemical mechanisms had striking biases that can be explained by either modeling assumptions or updates to the kinetic literature. The CB05 mechanism had by far the highest bias for organic nitrates (RNO_3), which can be explained by its representation of acetone. Both GEOS-Chem and RACM2 oxidized peroxy acetic acid much faster than the other chemical mechanisms, which can be explained by the choice of kinetic surrogate. All mechanisms overpredict peroxy nitric acid during the *young* age group, which can be improved by updating the $OH^\bullet$ rate constant. Each of these issues is explored in detail below, and implemented to see the change in estimated air parcel lifetime ($\overline{\tau_{air}}$).

The CB05 simulations partition up to 25% of total nitrogen into RNO_3, but all chemical mechanisms that explicitly represent acetone predict less than 3%. The RNO_3 production is a sink for both HO_x and NO_x, decreasing availability of $OH^\bullet$ and NO_2, which

ACPD
10, 20125–20165, 2010

leads to CB05 predicting the lowest HNO_3. The overprediction of RNO_3 by CB05 is a result of structural lumping that combines acetone into the model species PAR. The CB05 PAR species holds all singly bonded carbon, but also holds all carbon from acetone (Yarwood et al., 2005). Acetone has a long lifetime and high mixing ratios in the upper troposphere, so it can dominate the carbon in PAR (see Fig. 6). The PAR+$OH^{\bullet}$ organic nitrate yield, however, is based on urban, surface PAR reactivity (i.e., primarily alkanes). In CB05, the PAR+OH reaction creates an operator species (XO_2N), directly (13%) and indirectly (3%), that yield >10% organic nitrates production. In contrast, explicit representation of acetone in GEOS-Chem yields 3.6% organic nitrates. In the upper troposphere where acetone is the dominant PAR contributor, the organic nitrate fraction would have to be adjusted or acetone would need to be handled explicitly. A simple adjustment in CB05 of organic nitrate yield to 3% (as in GEOS-Chem) improves organic nitrate yield significantly and increases the $\overline{\tau_{air}}$ to 40 h, which is also the lower bound back trajectory $\overline{\tau_{air}}$ estimate.

GEOS-Chem and RACM2 predict a median peroxy acetic acid ($CH_3C(O)OOH$) mixing ratio less than the observed 25th percentile by the *young* age group. Peroxy acetic acid is the second largest acyl peroxy radical source (i.e., PAN precursor) in the first 6 h of simulated aging. The primary loss pathway for peroxy acetic acid is reaction with $OH^{\bullet}$, but the $OH^{\bullet}$ rate coefficient is not available in the literature. Both chemical mechanisms that underpredict peroxy acetic acid choose methyl peroxide as a surrogate compound for the $OH^{\bullet}$ rate coefficient. The chemical mechanisms that perform better, however, use the acetic acid $OH^{\bullet}$ rate coefficient. At upper tropospheric temperature and pressure, the acetic acid rate coefficient reported by Sander et al. (2006) (not updated from 2003 report see errata) and Atkinson et al. (2006) are both roughly ten times lower than the methyl peroxide $OH^{\bullet}$ rate. Preliminary peroxy acetic acid $OH^{\bullet}$ rate studies confirm the $k_{OH^{\bullet}}$ similarity to $CH_3C(O)OH$ (Orlando and Tyndall, 2002, private communication).

Pernitric acid is overpredicted by all chemical mechanisms and acts as an important radical sink in the upper troposphere. In the upper troposphere, pernitric acid

ACPD
10, 20125–20165, 2010

that is formed ($HO_2^{\bullet}+NO_2 \rightarrow HO_2NO_2$) is thermally stable, and the primary loss is $OH^{\bullet}+HO_2NO_2$ (see Fig. 7). The net pernitric acid reaction consumes two HO_x radicals (Wennberg et al., 1998) and, in this study, this net reaction accounts for 29% of the radicals terminated in the first 6 h. We recommend using the latest $k_{OH+HO_2NO_2}$ (Jimenez et al., 2004) which improves HO_2NO_2 agreement with observations and increases competition of pernitric acid with NO_2 for $OH^{\bullet}$ radicals. Even with this recommendation, the pernitric acid reaction rates have large uncertainties at low temperatures and laboratory studies are restricted to temperatures above those typical in the upper troposphere (Atkinson et al., 2004; Gierczak et al., 2005; Sander et al., 2006).

The peroxy acetic acid and peroxy nitrate recommendations implemented together into our working version of GEOS-Chem. These changes improve peroxy acetic acid and pernitric acid predictions, and increase the $\overline{\tau_{air}}$ estimate from 32 to 34 h. The new predicted NO_x:HNO_3 is now statistically consistent with observations at the $p<0.01$ level. Despite the improved NO_x:HNO_3, the $\overline{\tau_{air}}$ estimate is still 6 h shorter than the lowest back trajectory estimate, and the marginally longer $\overline{\tau_{air}}$ has little affect on long-lived carbon.

4 Discussion

The evidence gathered here suggests that the chemical mechanisms photochemically age NO_x too quickly. First, all chemical mechanism estimates of air parcel lifetime, the time necessary to age NO_x, are at least 15% shorter than the shortest back trajectory estimate. Second, the chemical mechanism air parcel lifetime estimates are insufficient to remove long-lived carbon, as seen in observations. Given these discrepancies, we conclude that chemical mechanisms will be low-biased for NO_x in the upper troposphere at any given time since convection.

We investigated individual chemical mechanism biases to develop and test recommendations. Peroxy acetic acid, a peroxy acetyl nitrate precursor, is removed too quickly by chemical mechanisms that use methyl peroxide; we recommend all mechanisms use acetic acid as a surrogate until a specific rate is available. Peroxy nitrates are an important radical sink in the upper troposphere, and we recommend several updates. The primary peroxy nitrate loss reactions in the upper troposphere are photolysis and hydroxyl attack. For photolysis, we recommend that all chemical mechanisms include photolysis for PANs and pernitric acid, and that pernitric acid near IR photolysis be included. For hydroxyl attack, we recommend updating the $OH^{\bullet}$ reaction rate (Jimenez et al., 2004). Finally, explicit or targeted parameterization of acetone is necessary to properly model radical cycling in the upper troposphere. Improved representation of acetone will decrease overpredictions of alkyl nitrates, which will alter radical cycling and total oxidation. The recommendations improved target species predictions and increased air parcel lifetime, but did not solve overpredictions of long-lived carbon.

This analysis included only gas-phase chemistry and ignores heterogeneous processing that also affects the NO_x:HNO_3 ratio. Including N_2O_5 heterogeneous hydrolysis would exacerbate the rate of NO_x to HNO_3 conversion (Jaeglé et al., 1998; Olson et al., 2001; Evans and Jacob, 2005). Mineral dust and ice particle uptake of HNO_3 would buffer or counteract the effect of N_2O_5 hydrolysis. Our initial analysis of HNO_3 uptake suggests that this rate would be small compared to nitric acid production NO_2+$OH^{\bullet}$. We intend to evaluate heterogeneous processing in more depth along chemical rate analysis there.

During this study, several best practices for atmospheric chemical modeling became apparent. The chemical system is very sensitive to the photolysis rates, and so it is critical to simulate photolysis in a detailed way when evaluating the chemical mechanisms. Photolysis simulations need to represent up-to-date pressure/temperature sensitivities. For instance, two models evaluated for use in this study did not include temperature/pressure sensitivities, which are critical in the upper troposphere. To accurately simulate temperature/pressure sensitivities, photolysis rates need to be calculated at the chemical transport model vertical resolution. Photolysis rates of many species (e.g. ozone) exhibit complex shape throughout the troposphere and linear interpolation can drastically underpredict local minima and maxima. Coarse resolution in some photolysis preprocessors is most likely a hold over from historically coarser CTM vertical resolutions. Also, ensure that the chemical mechanism used accounts for PAN photolysis and near-IR HO_2NO_2 photolysis. Photolysis is the dominant PAN chemical loss process in the upper troposphere, where many have reported PAN overprediction (Pickering et al., 2009; Yu et al., 2010; Fang et al., 2010).

5 Conclusions

This study uses a new probabilistic approach to isolate simulated chemistry for evaluation in the upper troposphere. This approach uses a large number of observations for statistical power and parameterizes processes whose stochastic nature precludes box model simulation. Parameterizing all other processes isolates gas-phase chemistry and produces an ideal modeling system for evaluation in the upper troposphere. Other upper troposphere gas-phase evaluations rely on steady-state assumptions or quasi-Lagrangian measurements. Steady-state assumptions may not be valid in the upper troposphere because convective mixing constantly perturbs NO_x and radical mixing ratios (Prather and Jacob, 1997). Quasi-Lagrangian analysis provides a direct evaluation approach when sufficient observations are available and their Lagrangian nature can be confirmed. Both the quasi-Lagrangian approach and our probabilistic approach have benefits that can complement each other to strengthen our body of knowledge where time-series observations from a single air parcel (e.g. smog chamber experiments) are not available.

One specific goal of this study was to characterize the contribution of chemistry to upper troposphere underprediction of NO_2. The results presented here confirm previously reported NO_2 underpredictions, and do so in an isolated chemistry model. All evaluated chemical mechanisms converted NO_x to HNO_3 too rapidly and, consequently, underpredicted NO_2 by at least 30%. Even if all emissions, physical transport, and aqueous-phase chemistry were accurately simulated by a chemical transport model, gas-phase chemistry would cause model underpredictions of NO_2.

This paper isolates chemistry and establishes NO_2 bias caused by chemistry. While this work does not resolve the problem, the modeling framework described provides an test environment for further analysis. Initial analyses demonstrate that results presented here are robust to uncertainty in initial conditions, but that rate expression uncertainty can meaningfully slow chemical mechanism NO_x aging. Future research will conduct sensitivity tests to identify key rate expressions. The results from subsequent sensitivity tests should be used to direct gas-phase rate research that will improve state of the science chemical mechanisms.

Appendix A

A1 Observation

The spatial distribution of all age groups (defined in the paper) are shown in Fig. 8.

A2 Subsequent convection

Upper troposphere air parcel lifetimes are limited by subsequently encountered convection and, so are exponentially distributed. Air parcels in the UT subside along isentropic surfaces, but not as rapidly as they are removed by convection related downdrafts (Prather and Jacob, 1997; Jaeglé et al., 1998). The importance of convection is most clear in the tropics where convection is very frequent. To confirm the importance of convection during the INTEX-NA, we simulated back trajectories a 12 locations forming a grid over the Northeastern United States using the Hybrid Single Particle Lagrangian Integrated Trajectory Model (HYSPLIT Draxler and Hess, 1997). During a 84 h (70% of the time between INTEX-NA convective events (Fuelberg et al., 2007)) back trajectory with only isentropic vertical motion, Fig. 9 shows that only 3 of the 12 simulations originated below 8 km or above 10 km. This confirms our conceptual model of convection as the dominant removal process of air parcels from the upper troposphere.

ACPD
10, 20125–20165, 2010

A3 Alternate background mixing scenarios

Our analysis uses background mixing calculated by Bertram et al. (2007), but there are significantly higher literature values. We test the sensitivity of our analysis by scaling our mixing parameter by 2, 4, and 10. Standard mixing is 5% per day, so these scaling values evaluate to 10%, 20%, and 50%. Twenty percent is the upper bound of values found in the literature (Bertram et al., 2007, and references therein) and 50% is used to demonstrate the influence of drastically increasing mixing. We also test the possibility of variable mixing efficiency and variable boundary conditions. This dynamic mixing test (DynMix) has mixing efficiency of 50% per day in the *initial* age group, 25% per day in the *fresh* age group, and 5% in *midage* and *old* age groups. These *initial* and *fresh* air parcels vigorously mix in chemical mixing ratios set by the air parcel's initial conditions. When the air parcel transitions to *young* age status, I decrease the mixing to 5x (also tried 6x) and start mix (1:1) of initial and background air, where background air is the average mixing ratio of all observations. When the air parcel transitions to *midage*, I return to the standard mixing rate and mix in "background" air. This is an extreme assumption because surrounding parcels should also be aging during the *fresh* time period.

Acknowledgements. Special thanks for DC8 observational data to Melody Avery, Donald Blake, William Brune, Alan Fried, Brian Heikes, Greg Huey, Glen Sachse, Hanwant Singh, and the INTEX team. Thank you to Paul Wennberg for helpful conversation about the upper troposphere. Thank you to Gao Chen for helping identify and document the INTEX HO_x corrections. Thank you to Mat Evans for help with the Dynamically Simple Model of Atmospheric Chemical Complexity.

This research was supported in part by an appointment to the Research Participation Program at the National Exposure Research Laboratory, US Environmental Protection Agency administered by the Oak Ridge Institute for Science and Education through an interagency agreement between the US Department of Energy and EPA.

In addition to the EPA program William R. Stockwell was supported in part by the NOAA Educational Partnership Program with Minority Serving Institutions (EPP/MSI) under grant number of

NA06OAR4810172 through the NOAA Center for Atmospheric Sciences (NCAS) and National Science Foundation grant award number: 0653997.

Askar Fahr thanks NASA-Outer Planets Research Program for partial support of this work under Contract #NNX08AQ68G at Howard University.

Disclaimer: Although this paper has been reviewed by the EPA and approved for publication, it does not necessarily reflect EPA's policies or views.

References

Atkinson, R., Baulch, D. L., Cox, R. A., Crowley, J. N., Hampson, R. F., Hynes, R. G., Jenkin, M. E., Rossi, M. J., and Troe, J.: Evaluated kinetic and photochemical data for atmospheric chemistry: Volume I – gas phase reactions of O_x, HO_x, NO_x and SO_x species, Atmos. Chem. Phys., 4, 1461–1738, doi:10.5194/acp-4-1461-2004, 2004. 20143

Atkinson, R., Baulch, D. L., Cox, R. A., Crowley, J. N., Hampson, R. F., Hynes, R. G., Jenkin, M. E., Rossi, M. J., Troe, J., and IUPAC Subcommittee: Evaluated kinetic and photochemical data for atmospheric chemistry: Volume II – gas phase reactions of organic species, Atmos. Chem. Phys., 6, 3625–4055, doi:10.5194/acp-6-3625-2006, 2006. 20142

Bertram, T. H., Perring, A. E., Wooldridge, P. J., Crounse, J. D., Kwan, A. J., Wennberg, P. O., Scheuer, E., Dibb, J., Avery, M. A., Sachse, G. W., Vay, S. A., Crawford, J. H., McNaughton, C. S., Clarke, A., Pickering, K. E., Fuelberg, H., Huey, G., Blake, D. R., Singh, H. B., Hall, S. R., Shetter, R. E., Fried, A., Heikes, B. G., and Cohen, R. C.: Direct measurements of the convective recycling of the upper troposphere, Science, 315, 816–820, doi:10.1126/science.1134548, 2007. 20126, 20127, 20128, 20130, 20132, 20135, 20147, 20154

Carter, W. P.: Documentation of the SAPRC-99 Chemical Mechanism for VOC Reactivity Assessment, final report to California Air Resources Board, Contract 92-329 and 95-308, Calif. Air Res. Board, Sacramento, CA, USA, 2000. 20133

Carter, W. P.: Development of the SAPRC-07 Chemical Mechanism and Updated Ozone Reactivity Scales, Final Report to the California Air Resources Board Contract No. 03-318, Calif. Air Res. Board, Sacramento, CA, USA, http://www.engr.ucr.edu/~carter/SAPRC/saprc07.pdf, 2009. 20133

Dodge, M.: Chemical oxidant mechanisms for air quality modeling: critical review, Atmos. Environ., 34, 2103–2130, 2000. 20129
Draxler, R. and Hess, G.: Description of the HYSPLIT 4 modeling system, NOAA Technical Memorandum ERL ARL-224, p. 24, 1997. 20146
Emmerson, K. M. and Evans, M. J.: Comparison of tropospheric gas-phase chemistry schemes for use within global models, Atmos. Chem. Phys., 9, 1831–1845, doi:10.5194/acp-9-1831-2009, 2009. 20132
Emmons, L., Walters, S., Hess, P., Lamarque, J., Pfister, G., Fillmore, D., Granier, C., Guenther, A., Kinnison, D., Laepple, T., Orlando, J., Tie, X., Tyndall, G., Wiedinmyer, C., Baughcum, S., and Kloster, S.: Description and evaluation of the Model for Ozone and Related chemical Tracers, version 4 (MOZART-4), Geosci. Model Develop., 3, 43–67, 2010. 20133
Evans, M. and Jacob, D.: Impact of new laboratory studies of N_2O_5 hydrolysis on global model budgets of tropospheric nitrogen oxides, ozone, and OH, Geophys. Res. Lett, 32, 1–4, 2005. 20144
Eyers, C., Norman, P., Middel, J., Plohr, M., Michot, S., Atkinson, K., and Christou, R.: AERO2k Global Aviation Emissions Inventories for 2002 and 2025, 2004. 20127
Fang, Y., Fiore, A., Horowitz, L., Levy II, H., Hu, Y., and Russell, A.: Sensitivity of the NO_y budget over the United States to anthropogenic and lightning, J. Geophys. Res., doi:10.1029/2010JD014079, in press, 2010. 20145
Fuelberg, H. E., Porter, M. J., Kiley, C. M., Halland, J. J., and Morse, D.: Meteorological conditions and anomalies during the Intercontinental Chemical Transport Experiment – North America, J. Geophys. Res., 112, 1–22, doi:10.1029/2006JD007734, 2007. 20136, 20146
Gallager, R. G.: Discrete Stochastic Processes, Kluwer Academic Publishers, Boston Dordrecht London, 1996. 20135
Gierczak, T., Jimenez, E., Riffault, V., and Burkholder, J.: Thermal decomposition of HO_2NO_2 (peroxynitric acid, PNA): Rate coefficient and Determination of the Enthalpy of Formation, J. Phys. Chem., 109, 586–596, http://pubs.acs.org/doi/abs/10.1021/jp046632f, 2005. 20143
Goliff, W., Stockwell, W., and Fahr, A.: The Regional Atmospheric Chemistry Mechanism, Version 2, in preparation, 2010. 20133
Goliff, W. S. and Stockwell, W. R.: The Regional Atmospheric Chemistry Mechanism, Version 2 An Update, in: Atmospheric Chemical Mechanisms, University of California Davis, 2008. 20133
Hudman, R., Jacob, D., Turquety, S., Leibensperger, E., Murray, L., Wu, S., Gilliland, A., Av-

ery, M., Bertram, T., Brune, W., Cohen, R., Dibb, J., Flocke, F., Fried, A., Holloway, J., Neuman, J., Orville, R., Perring, A., Ren, X., Sachse, G., Singh, H., Swanson, A., and Wooldridge, P.: Surface and lightning source of nitrogen oxides over the United States: Magnitudes, chemical evolution, and outflow, J. Geophys. Res., 112, D12S05, doi:10.1029/2006JD007912, 2007. 20127, 20128

Jaeglé, L., Jacob, D., Wang, Y., and Weinheimer, A.: Sources and chemistry of NO_x in the upper troposphere over the United States, Geophys. Res. Lett., 25(10), 1709–1712, http://citeseerx.ist.psu.edu/viewdoc/download?doi=10.1.1.6.7937&rep=rep1&type=pdf, 1998. 20144, 20146

Jimenez, E., Gierczak, T., Stark, H., and Burkholder, J.: Reaction of OH with HO_2NO_2 (Peroxynitric Acid): Rate coefficients between 218 and 335 K and product yields at 298 K, J. Phys. Chem., 108, 1139–1149, http://pubs.acs.org/doi/abs/10.1021/jp0363489, 2004. 20143, 20144

Lacis, A., Wuebbles, D., and Logan, J.: Radiative forcing of climate by changes in the vertical distribution of ozone, J. Geophys. Res., 95, 9971–9982, 1990. 20127

Madronich, S.: The Tropospheric Visible Ultra-violet (TUV) model web page., http://www.acd.ucar.edu/TUV/, 2002. 20133

Mann, H. and Whitney, D.: On a test of whether one of two random variables is stochastically larger than the other, Ann. Math. Stat., 18, 50–60, 1947. 20138

Mao, J., Carouge, C., Evans, M., Millet, D., and Palmer, P.: GEOS-Chem Chemical Mechanism Version 8-02-04, http://acmg.seas.harvard.edu/geos/wiki_docs/chemistry/chemistry_updates_v6.pdf, 2009. 20133

Murphy, J. G., Thornton, J. A., Wooldridge, P. J., Day, D. A., Rosen, R. S., Cantrell, C., Shetter, R. E., Lefer, B., and Cohen, R. C.: Measurements of the sum of HO_2NO_2 and $CH_3O_2NO_2$ in the remote troposphere, Atmos. Chem. Phys., 4, 377–384, doi:10.5194/acp-4-377-2004, 2004. 20134

Napelenok, S. L., Pinder, R. W., Gilliland, A. B., and Martin, R. V.: A method for evaluating spatially-resolved NO_x emissions using Kalman filter inversion, direct sensitivities, and space-based NO_2 observations, Atmos. Chem. Phys., 8, 5603–5614, doi:10.5194/acp-8-5603-2008, 2008. 20126, 20127

Olson, J., Crawford, J., Davis, D., Chen, G., Avery, M., Barrick, J., Sachse, G., Vay, S., Sandholm, S., and Tan, D.: Seasonal differences in the photochemistry of the South Pacific: a comparison of observations and model results from PEM-Tropics A and B, J. Geophys.

Discussion Paper | Discussion Paper | Discussion Paper | Discussion Paper |

ACPD

10, 20125–20165, 2010

Upper tropospheric NO_y evaluation

B. H. Henderson et al.

Res., 106, 32749, 2001. 20144

Olson, J. R., Crawford, J., Chen, G., Brune, W. H., Faloona, I. C., Tan, D., Harder, H., and Martinez, M.: A reevaluation of airborne HO_x observations from NASA field campaigns, J. Geophys. Res.-Atmos., 111, D10301, doi:10.1029/2005JD006617, 2006. 20126, 20128, 20138

Orlando, J. and Tyndall, G.: Fall Meet. Suppl., Abstract A61B-0078, Eos Trans. AGU, 83, 2002. 20142

Pickering, K., Pinder, R., Prados, A., Allen, D., Stehr, J., Dickerson, R., Ehrman, S., Szykman, J., Celarier, E., and Gleason, J.: Use of OMI Data in Monitoring Air Quality Changes Resulting from NO_x Emission Regulations over the United States, 2009 CMAS Conference, 1–19, 2009. 20127, 20145

Prather, M. and Jacob, D.: A persistent imbalance in HO_x and NO_x photochemistry of the upper troposphere driven by deep tropical convection, Geophys. Res. Lett., 24, 3189–3192, 1997. 20145, 20146

Real, E., Law, K. S., Schlager, H., Roiger, A., Huntrieser, H., Methven, J., Cain, M., Holloway, J., Neuman, J. A., Ryerson, T., Flocke, F., de Gouw, J., Atlas, E., Donnelly, S., and Parrish, D.: Lagrangian analysis of low altitude anthropogenic plume processing across the North Atlantic, Atmos. Chem. Phys., 8, 7737–7754, doi:10.5194/acp-8-7737-2008, 2008. 20128

Ren, X., Olson, J. R., Crawford, J. H., Brune, W. H., Mao, J., Long, R. B., Chen, Z., Chen, G., Avery, M. A., Sachse, G. W., BARRICK, J. D., Diskin, G. S., Huey, L. G., Fried, A., Cohen, R. C., Heikes, B. G., Wennberg, P. O., Singh, H. B., Blake, D. R., and Shetter, R. E.: HO_x chemistry during INTEX-A 2004: observation, model calculation, and comparison with previous studies, J. Geophys. Res., 113, 1–13, doi:10.1029/2007JD009166, 2008. 20126, 20128, 20154

Sander, S., Friedl, R. R., Golden, D. M., Kurylo, M. J., Moortgat, G. K., Wine, P. H., Ravishankara, A. R., Kolb, C. E., Molina, M. J., Finlayson-Pitts, B. J., Huie, R. E., and Orkin, V.: Chemical Kinetics and Photochemical Data for Use in Atmospheric Studies Evaluation Number 15, JPL Publ., 2006. 20142, 20143

Sandu, A. and Sander, R.: KPP-2.1 User's Manual The Kinetic PreProcessor KPP An Environment for the Simulation of Chemical Kinetic Systems, 1–29, 2005. 20132

Saunders, S., Jenkin, M., and Derwent, R.: Report summary: web site of a Master Chemical Mechanism (MCM) for use in tropospheric chemistry models, Atmos. Environ., 31, 1249, doi:10.1016/S1352-2310(97)85197-7, 1997. 20133

Scholz, F. and Stephens, M.: K-sample Anderson-Darling tests, J. Am. Stat. Assoc., 82(399), 918–924, 1987. 20137

Singh, H. B., Brune, W. H., Crawford, J., Jacob, D. J., and Russel, P.: Overview of the summer 2004 Intercontinental Chemical Transport Experiment – North America (INTEX-A), J. Geophys. Res, 111, 17, doi:10.1029/2006JD007905, 2006. 20128, 20131

Singh, H. B., Salas, L., Herlth, D., Kolyer, R., Czech, E., Avery, M. A., Crawford, J., Pierce, R., Sachse, G. W., Blake, D. R., Cohen, R. C., Bertram, T. H., Perring, A. E., Wooldridge, P. J., Dibb, J., Huey, G., Hudman, R., Turquety, S., Emmons, L., Flocke, F., Tang, Y., Carmichael, G., and Horowitz, L.: Reactive nitrogen distribution and partitioning in the North American troposphere and lowermost stratosphere, J. Geophys. Res, 112, D12S04, doi:10.1029/2006JD007664, 2007. 20126, 20127, 20131

Stockwell, W. R., Goliff, W. S., Pinder, R. W., Sarwar, G., Mathur, R., Schere, K. L., and Fahr, A.: A model comparison of nitrogen-containing compounds in the free troposphere using three mechanisms: RACM2, CB05 and SAPRC99, in: Eos Trans. AGU, vol. 89(53) of Fall Meet. Suppl., Abstract A54C–08, 2008. 20133

Sutkus, D., Baughcum, S., and DuBois, D.: Commercial aircraft emission scenario for 2020: Database Development and Analysis, National Aeronautics and Space Administration, Glenn Research Center, Washington, 2003. 20127

Wennberg, P., Hanisco, T., Jaegle, L., Jacob, D., Hintsa, E., Lanzendorf, E., Anderson, J., Gao, R.-S., Keim, E., Donnelly, S., Negro, L. D., Fahey, D., McKeen, S., Salawitch, R., Webster, C., May, R., Herman, R., Proffitt, M., Margitan, J., Atlas, E., Schauffler, S., Flocke, F., McElroy, C., and Bui, T.: Hydrogen radicals, nitrogen radicals, and the production of O_3 in the upper troposphere, Science, 279, 49–53, doi:10.1126/science.279.5347.49, 1998. 20143

Wild, O., Zhu, X., and Prather, M. J.: Fast-J: accurate simulation of in-and below-cloud photolysis in tropospheric chemical models, J. Atmos. Chem., 37, 245–282, http://www.springerlink.com/index/Q532038171841385.pdf, 2000. 20133

Yarwood, G., Yocke, M., and Whitten, G. Z.: Updates to the Carbon Bond Chemical Mechanism: CB05, http://camx.com/publ/pdfs/CB05_Final_Report_120805.pdf, 2005. 20133, 20142

Yu, S., Mathur, R., Sarwar, G., Kang, D., Tong, D., Pouliot, G., and Pleim, J.: Eta-CMAQ air quality forecasts for O_3 and related species using three different photochemical mechanisms (CB4, CB05, SAPRC-99): comparisons with measurements during the 2004 ICARTT study, Atmos. Chem. Phys., 10, 3001–3025, doi:10.5194/acp-10-3001-2010, 2010. 20145

Table 1. Overview of chemical mechanisms in this study.

Chemical Mechanism (abbreviation)	# Rxns	# Spcs
Carbon Bond ’05 (CB05)	176	62
State Air Pollution Research Center ’99 (SAPRC99)	222	77
State Air Pollution Research Center ’07 (SAPRC07)	691	153
Model for OZone And Related chemical Tracers “Standard” (MZ4)	196	86
GEOS-Chem “full” (GEOS-Chem)	286	88
Regional Atmospheric Chemistry Mech v.2 (RACM2)	349	117
Master Chemical Mechanism Active Subset (MCM)	4685	1610

ACPD
10, 20125–20165, 2010

Table 2. Median observed values for filtered *initial* (n_i=108) and *background* (n_{bkg}=1006) selected chemical compounds and physical conditions.

Measured	Background	Initial	Principal Invesitigator
Altitude	8841 m	9149 m	J. Barrick, NASA LaRC
Pressure	314.7 hPa	300.6 hPa	
Temperature	241.1 K	233.7 K	
$HO^\bullet$	0.5396 pptv	0.6101 pptv	W. Brune, Pennsylvania State University; Adjusted according to Ren et al. (2008)
$HO_2^\bullet$	13.16 pptv	11.24 pptv	
O_3	77.76 ppbv	70.61 ppbv	M. Avery, NASA LaRC
NO_2	95.52 pptv	153.6 pptv	R. Cohen, UC Berkeley
NO	203.3 pptv	411.8 pptv	Derived from NO_2, O_3, and HO_2
HNO_3	280.1 pptv	125.9 pptv	P. Wennberg, California Institute of Technology; R. Talbot, Univ. of New Hampshire; Adjusted following Bertram et al. (2007)
HO_2NO_2	82.00 pptv	67.80 pptv	G. Huey, Georgia Institute of Technology
H_2O_2	234.2 pptv	195.9 pptv	P. Wennberg, California Institute of Technology; B. Heikes, Univ. of Rhode Island; Adjusted following Bertram et al. (2007)
CO	98.36 ppbv	108.0 ppbv	G. Sachse, NASA LaRC
CH_4	1.789 ppmv	1.784 ppmv	D. Blake, UC Irvine, and E. Atlas Univ. of Miami
C_2H_6	790.0 pptv	800.0 pptv	
C_3H_8	146.0 pptv	153.5 pptv	
C_2H_4	1.500 pptv	1.500 pptv	
Speciated alkyl nitrates (RNO_3)	8.630 pptv	8.630 pptv	
CH_2O	174.5 pptv	437.0 pptv	A. Fried, NCAR; B. Heikes, Univ. of Rhode Island
$CH_3C(O)H$	83.80 pptv	117.5 pptv	H. Singh, NASA ARC
$CH_3C(O)CH_3$	1475. pptv	1375. pptv	
$CH_3C(O)C_2H_5$	71.25 pptv	95.00 pptv	
PAN	374.9 pptv	370.6 pptv	
$CH_3C(O)OOH$	172.8 pptv	226.1 pptv	P. Wennberg, California Institute of Technology

ACPD
10, 20125–20165, 2010

Table 3. Optimization results for stochastic convection using the pure exponential model and the model with correction for preferential sampling. Table includes optimal air parcel lifetime ($\overline{\tau_{\text{air}}}$) and Anderson Darling goodness-of-fit test value (T_{kaN}) for alternative background mixing rate sensitivities. The predicted NO_x:HNO_3 is statistically different than observations when T_{kaN} is greater than 3.752 (α=0.01).

Mechanism	exponential $\overline{\tau_{\text{air}}}$	exponential T_{kaN}	corrected $\overline{\tau_{\text{air}}}$	corrected T_{kaN}
GEOS-Chem	23	9.9	33	2.77
2×Mix	21	10.6	32	3.62
4×Mix	20	11.6	31	5.59
10×Mix	18	15.9	28	10.2
GC*	24	8.32	36	2.28
M10×Init	28	65.9	43	51
DynMix	24	7.42	36	2.28

ACPD
10, 20125–20165, 2010

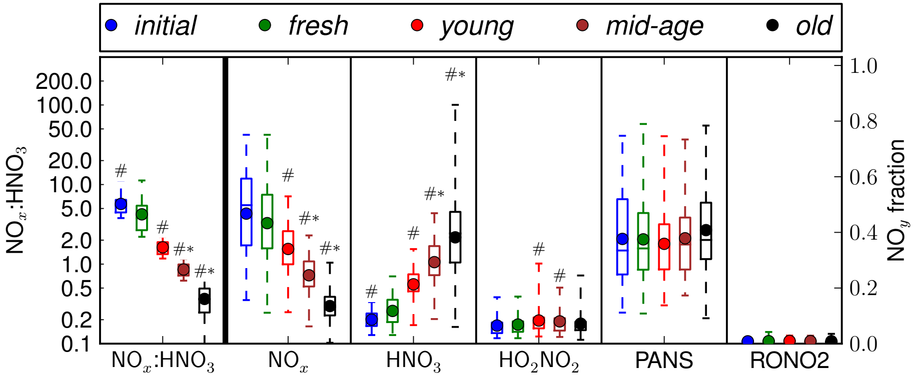

Fig. 1. Nitrogen partitioning of *fresh*, *young*, *midage* and *old* age categories demonstrates influence of chemical aging. Each age category has been tested for statistical difference ($p<0.0001$) from the preceding age category ($*$) and *fresh* (#).

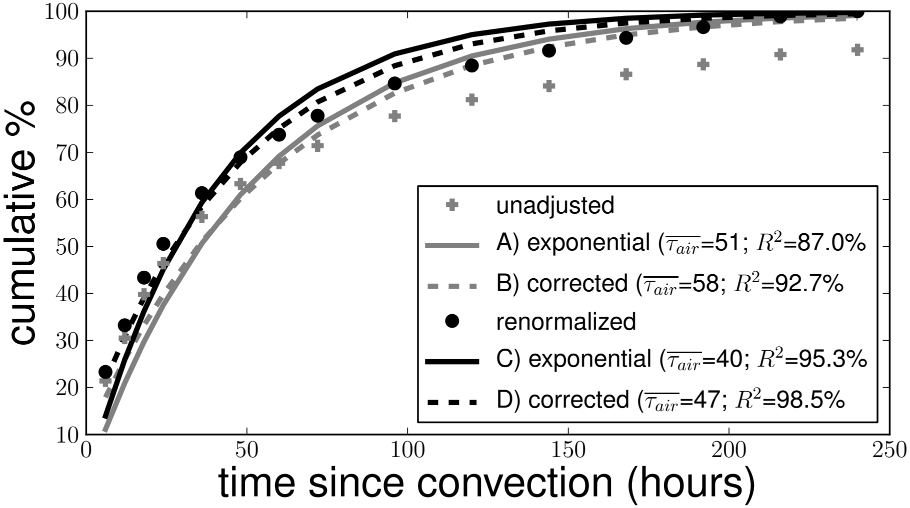

Fig. 2. Optimization results for stochastic convection using the exponential and bias-corrected statistical model with the unadjusted and renormalized back trajectory dataset. (A) exponential model (Eq. 1) with unadjusted dataset; (B) bias-corrected model (Eq. 2) with renormalized dataset; (C) exponential model with unadjusted dataset; (D) bias-corrected model with renormalized dataset.

ACPD
10, 20125–20165, 2010

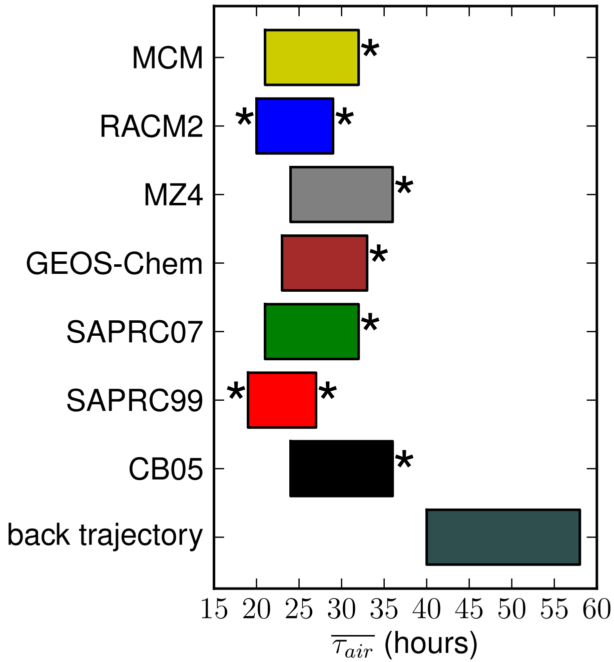

Fig. 3. Range of estimated mean air parcel lifetimes ($\overline{\tau_{air}}$) derived from back trajectory and chemical simulation. Asterisks indicate whether chemically simulated NO_x:HNO_3 is statistically consistent with observations (α<0.01) when using the exponential (left, Eq. 3) and bias-corrected (right, Eq. 4) statistical models.

ACPD
10, 20125–20165, 2010

ACPD
10, 20125–20165, 2010

Upper tropospheric NO_y evaluation

B. H. Henderson et al.

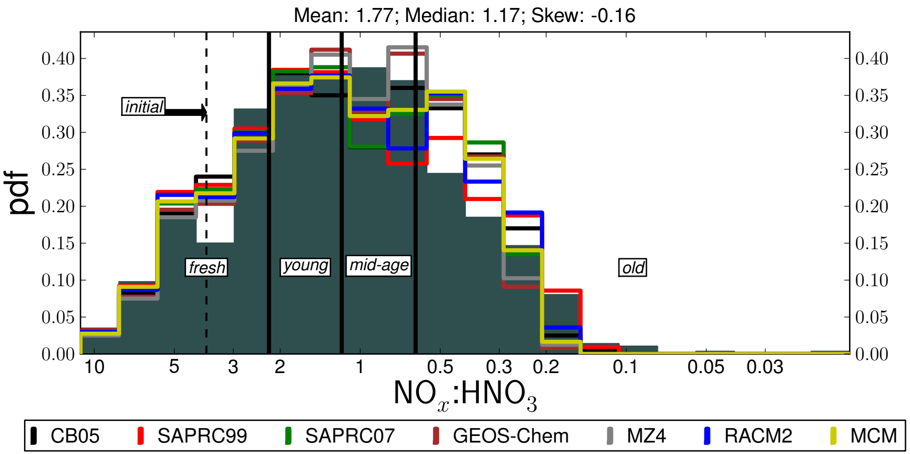

Fig. 4. Observed NO_x:HNO_3 (bars) compared to simulated (lines) from each chemical mechanism using the optimized, bias-corrected statistical model.

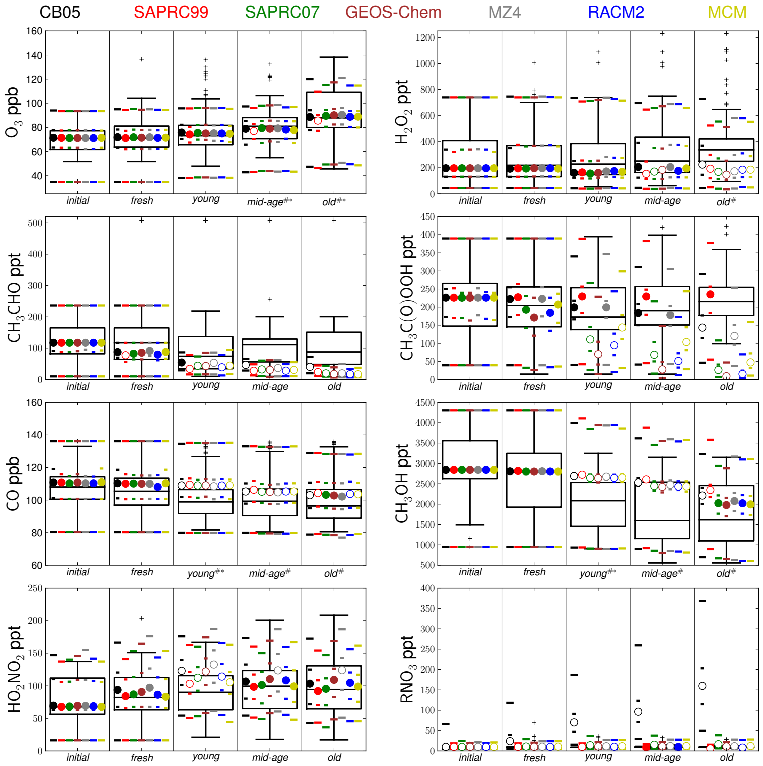

Fig. 5. Simulation results (circle: median; bars: 0, 25, 75, 100 percentiles) and observations (box and whisker) binned by NO_x:HNO_3. For observations, each age category is superscripted for statistical difference (p<0.0001) from the preceding (∗) and *fresh* (#) age group. For model predictions, the median for each chemical mechanism is left hollow when statistically different (p<0.0001) from the observations.

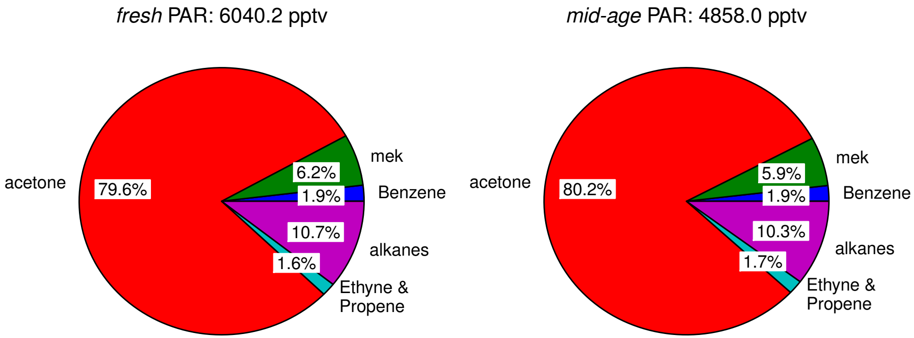

Fig. 6. Composition of CB05 PAR chemical mechanism species as measured during INTEX-NA in the *median* air parcel for *fresh* and *young* age groups.

ACPD
10, 20125–20165, 2010
Upper tropospheric NO_y evaluation
B. H. Henderson et al.

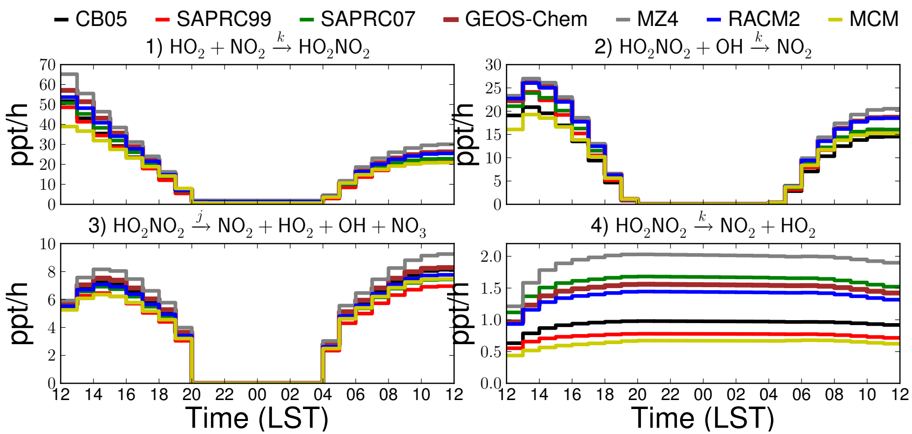

Fig. 7. Pernitric acid gross production and loss from the *median* air parcel.

ACPD
10, 20125–20165, 2010

Upper tropospheric NO_y evaluation

B. H. Henderson et al.

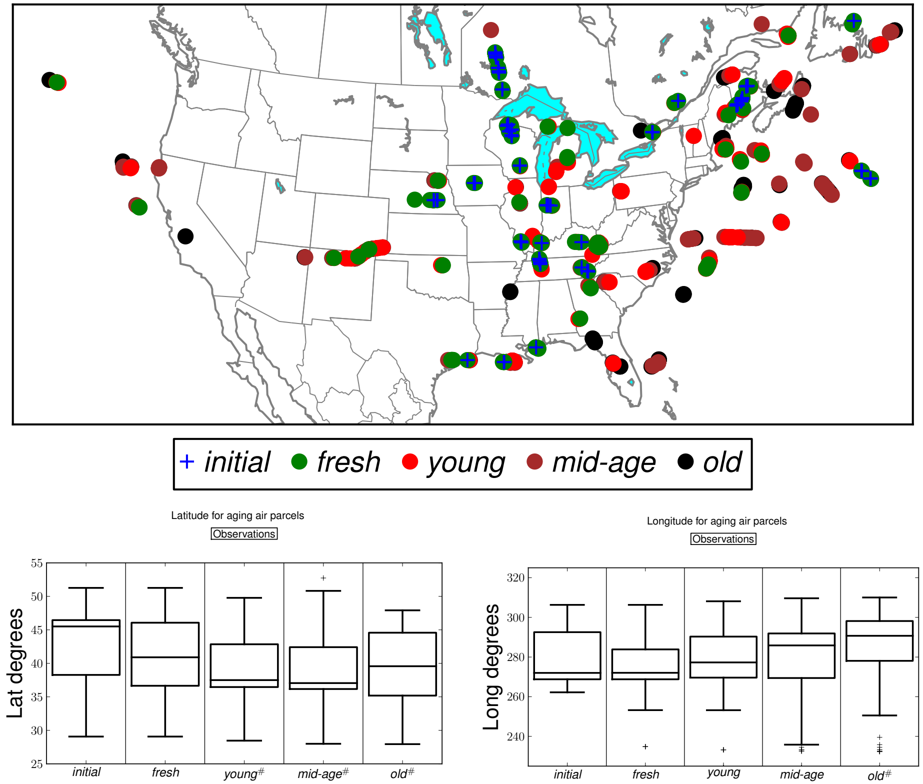

Fig. 8. Map **(a)** and distribution **(b,c)** of spatial locations of aircraft observations categorized by age groups (initial, fresh, young, mid-age, and old). Age group definitions are shown in Fig. 4.

ACPD
10, 20125–20165, 2010

Upper tropospheric NO_y evaluation

B. H. Henderson et al.

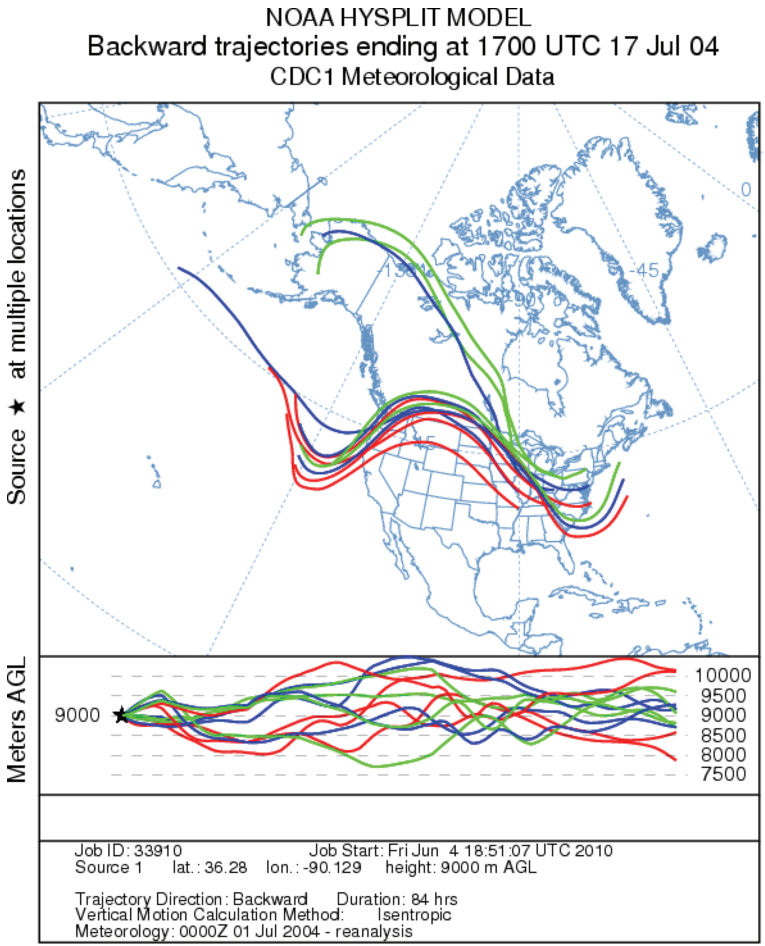

Fig. 9. HYSPLIT back trajectories for 12 northeast locations at 9 km altitude with only more than half of the air parcels originating between 8 and 10 km.

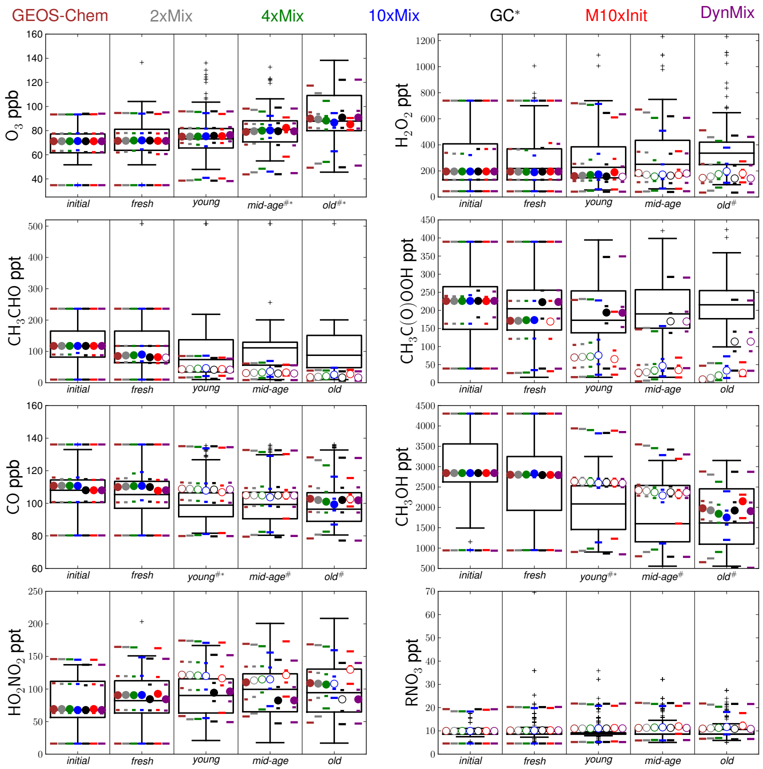

Fig. 10. Same as Fig. 5, but for GEOS-Chem with standard and alternate background mixing.

Discussion Paper | Discussion Paper | Discussion Paper | Discussion Paper |

ACPD

10, 20125–20165, 2010

Upper tropospheric NO_y evaluation

B. H. Henderson et al.